Materials Characterization 127 (2017) 371–378

Contents lists available at ScienceDirect

Materials Characterization

journal homepage: www.elsevier.com/locate/matchar

Effect of scandium on microstructure and mechanical properties of high zinc concentration aluminum alloys

W.B. Zhou[a,b], C.Y. Liu[c,d,*], P.F. Yu[e], B. Zhang[e], Z.Y. Ma[c], K. Luo[d,**], M.Z. Ma[e], R.P. Liu[e]

[a] College of Materials Science and Engineering, Beijing University of Technology, Beijing 100022, China
[b] Alnan Aluminium Co., Ltd., Nanning 530031, China
[c] Shenyang National Laboratory for Materials Science, Institute of Metal Research, Chinese Academy of Sciences, 72 Wenhua Road, Shenyang 110016, China
[d] Key Laboratory of New Processing Technology for Nonferrous Metal & Materials, Ministry of Education, Guilin University of Technology, Guilin 541004, China
[e] State Key Laboratory of Metastable Materials Science and Technology, Yanshan University, Qinhuangdao 066004, China

ARTICLE INFO

Keywords:
Microstructure
Hardness
Al alloy
Heat treatment

ABSTRACT

This study investigated the effect of Sc addition on the microstructure and mechanical properties of a high-Zn-concentration Al (Al–49Zn) alloy. The addition of 0.5Sc obviously refined the Al grains and Zn phases in the Al–49Zn alloy during solidification. It also suppressed the Al grain coarsening and Zn dissolution in the Al–49Zn alloy during heat treatment because of the pinning effect of nanoscale Al_3Sc precipitates and Sc atoms. Given its refined structure and high thermal stability, the Al–49Zn–0.5Sc alloy showed high hardness and mechanical stability after heating.

1. Introduction

The addition of rare-earth Sc into commercial Al alloys is an effective approach to improve their microstructure and mechanical properties. The primary Al_3Sc phase can serve as a heterogeneous nucleation site for Al grains during solidification and lead to grain refinement in Al alloys [1–3]. The extremely fine and coherent Al_3Sc precipitates that are obtained during homogenization treatment can significantly inhibit the dislocation and grain boundary (GB) motion in Al alloys during subsequent thermomechanical processes, thereby promoting dislocation and GB strengthening [2,4–6]. Thus, commercial Al alloys added with Sc are usually characterized by high strength [7–9], enhanced superplasticity [4,5,10], good welding performance [11], and excellent thermal stability [12,13].

Different from commercial Al alloys, Al–Zn alloys contain much higher solute concentrations (20%–45% mass fraction). Therefore, the Al crystal grows cooperatively with the second phase during solidification, and high-density Zn lamellae are observed in Al–Zn-based cast alloys [14,15]. Moreover, a much more prominent solid-solution hardening effect is achieved in the Al–Zn system than in commercial Al alloys after heat treatment [20]. A unique dynamic precipitation phenomenon is observed in Al–Zn-based alloys during cold deformations [15–20].

As mentioned above, the addition of Sc or high-concentration Zn obviously affects the solidification, solid solution, precipitation, and recrystallization in Al alloys. However, the synergistic effect of Sc and high-concentration Zn on the microstructure and mechanical properties of Al alloys remains unclear to date. Determining whether high solute content affects Sc addition-induced increases in grain refinement, GB pinning, and hardness in Al alloys is interesting. Li et al. [21] found that the Zn solution temperature can lead to the precipitation of a nanoscale Al_3Sc phase in the Al–Zn–Mg–Sc system and that no intermetallic compounds and interdiffusion exist between Sc and Zn. Thus, the interaction between Zn solid solution and Al_3Sc precipitation during heat treatment is a worthwhile area of study.

In the present study, Al–49Zn and Al–49Zn–0.5Sc alloys were subjected to microstructural examinations and hardness measurement under as-cast and heat treatment conditions. This study aims to understand the interaction between Sc addition and high-density Zn solute, as well as elucidate the effect of Sc on the solidification and thermal stability of high-Zn-concentration Al alloys. The results of this study could provide a basis for further material design in the Al–Zn–Sc–X system.

* Correspondence to: C.Y. Liu, Shenyang National Laboratory for Materials Science, Institute of Metal Research, Chinese Academy of Sciences, 72 Wenhua Road, Shenyang 110016, China.
** Corresponding author at: Key Laboratory of New Processing Technology for Nonferrous Metal & Materials, Ministry of Education, Guilin University of Technology, Guilin 541004, China
E-mail addresses: lcy261@glut.edu.cn (C.Y. Liu), luokun@glut.edu.cn (K. Luo).

http://dx.doi.org/10.1016/j.matchar.2017.03.028
Received 7 October 2016; Received in revised form 14 March 2017; Accepted 18 March 2017
Available online 20 March 2017
1044-5803/

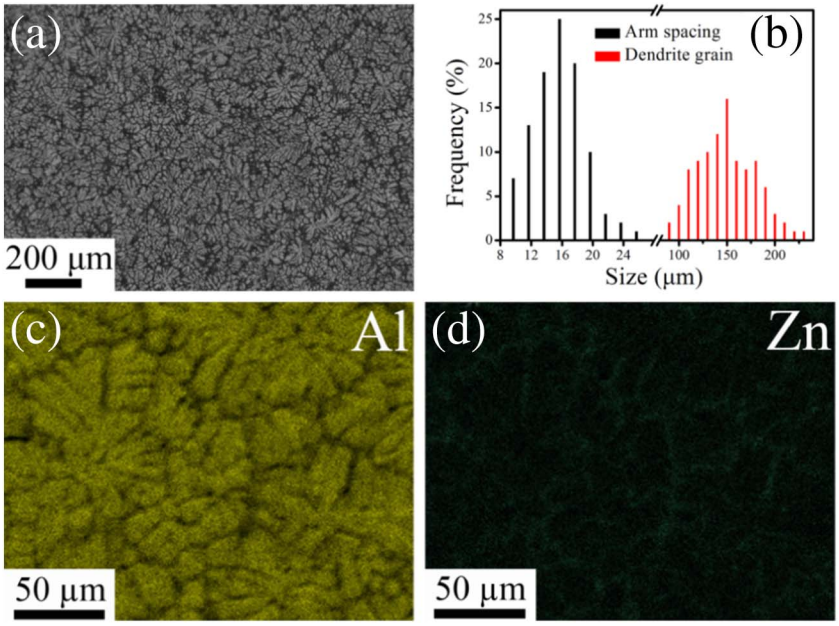

Fig. 1. (a) OM micrograph and (b) arm spacing and dendrite grain size distributions of the as-cast Al–49Zn alloy. The corresponding composition mapping of Al and Zn is shown in (c) and (d), respectively.

2. Experimental Methods

Al–49Zn and Al–49Zn–0.5Sc alloys were prepared by melting commercial pure Al (99.9%), pure Zn (99.9%), and Al–2%Sc (mass fraction) master alloy in a resistance heating furnace with a graphite crucible. The as-cast alloys were heated for 5 h and then quenched in water. Heat treatment was conducted at 300 °C, 400 °C, 450 °C, and 480 °C.

The microstructures of the alloys were examined via optical microscopy (OM), scanning electron microscopy (SEM), and transmission electron microscopy (TEM). The chemical composition of SEM specimens was characterized using energy-dispersive X-ray spectrometer (EDS). Films for TEM were prepared by grinding the alloy to a thickness of 30 μm and then ion-milling. The phases of the Al–49Zn and Al–49Zn–0.5Sc alloys were confirmed through X-ray diffraction (XRD). Hardness measurement was performed with a Vickers microhardness tester (using 3000 gf load for 15 s).

3. Results and Discussion

Fig. 1 shows the microstructure of the Al–49Zn alloy in the as-cast state. The alloy was characterized by a typical dendritic structure (Fig. 1(a)). The average sizes of the arm spacing and grain in the as-cast Al–49Zn alloy were approximately 16 and 150 μm, respectively, according to the size statistics (Fig. 1(b)). The solute segregation during casting produced high-concentration Zn in the interdendritic eutectic regions (Fig. 1(c) and (d)).

Fig. 2 shows the TEM micrographs of the as-cast Al–49Zn alloy. The white and gray regions correspond to the Al and Zn phases, respectively. A typical eutectic growth model was exhibited by the Al–Zn binary system. Zn lamellae with an average thickness of 80 nm were obtained in the Al matrix through the combination of the two shapes of the Zn phase.

The crystallization temperature of nearly 100 °C in the Al–49Zn alloy led to the formation of a typical dendritic structure (Fig. 1(a)). In the dendritic grain interior, the growth of Al-rich crystal resulted in the accumulation of rejected Zn atoms near the Al phase. The enrichment of Zn atoms promoted the nucleation and growth of the Zn phase in the neighboring regions of Al crystal. Thus, Zn lamellae were observed in the Al grains (Fig. 2).

Fig. 3 shows the SEM images of the Al–49Zn–0.5Sc alloy in the as-cast state. Dendritic and equiaxed structures of Al may be observed in this sample (Fig. 3(a)). The average size of equiaxed grains was approximately 41 μm, according to the size statistics (Fig. 3(b)). Zn segregation appeared along the Al GBs (Fig. 3(c) and (d)). However, the distribution of Sc was difficult to observe by mapping images because of the low density of this element (Fig. 3(e)).

Point analysis by EDS of the as-cast Al–49Zn–0.5Sc alloy is presented in Fig. 4. High Sc concentration was obtained near the GBs (Spots 1 and 3). The white regions between Al grains corresponded to the Zn phase, and the Sc content in the Zn phase was low (Spot 2). The Sc distribution in the Al grain interior was uniform, and the mass fraction was approximately 0.25% (Spots 4–6).

Fig. 5 shows the TEM micrographs of the as-cast Al–49Zn–0.5Sc alloy. The morphology, distribution, and size of the Zn phase exhibited distinct differences in the dendritic and equiaxed Al grains of this alloy (Fig. 5(a)). Region B, which corresponded to the interior of the dendritic grains, showed a similar microstructure to the as-cast Al–49Zn alloy (Fig. 2). Zn lamellae were also displayed in this region (Fig. 5(b)). Compared with the Zn phase in the dendritic grains, the second phase at the dendritic–equiaxed grain interface was much smaller (Fig. 5(c)). A higher density of the needle-like Zn phase, with a size of approximately 30 nm, was found in the equiaxed grains (Fig. 5(d)).

Clearly, minor Sc addition can change the morphology and size of Al grains and the Zn phase of the Al–49Zn alloy during solidification (Figs. 1–5).

For the Al–49Zn–0.5Sc alloy, two solidification modes occurred simultaneously. One mode is similar to that of the Al–49Zn alloy, and this mode promoted the formation of a dendritic structure in the as-cast Al–Zn–Sc alloy (Fig. 3). Compared with the Al–49Zn alloy, the Al–49Zn–0.5Sc alloy exhibited a higher supercooling degree during solidification because of the greater number of solute atoms in the latter. Karamazi et al. [22] showed that the eutectic spacing of the Al–Zn system decreases with increasing supercooling degree. This finding may explain why the size of the Zn phase in the dendritic structure was smaller than that of the as-cast Al–49Zn alloy (Fig. 5(b)). During the solidification of the dendritic structure in the Al–Zn–Sc alloy, the growth of the Zn phase maybe also suppressed by the high Sc solute concentration through the interdiffusion between Sc and Zn.

The other solidification mode was caused by the primary Al_3Sc

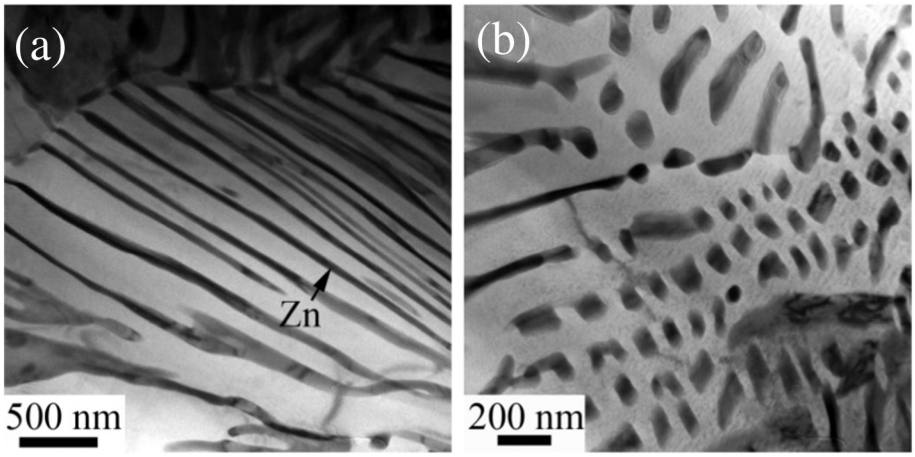

Fig. 2. TEM micrographs of the as-cast Al–49Zn alloy in different regions showing Zn phases with (a) fiber and (b) equiaxed shapes.

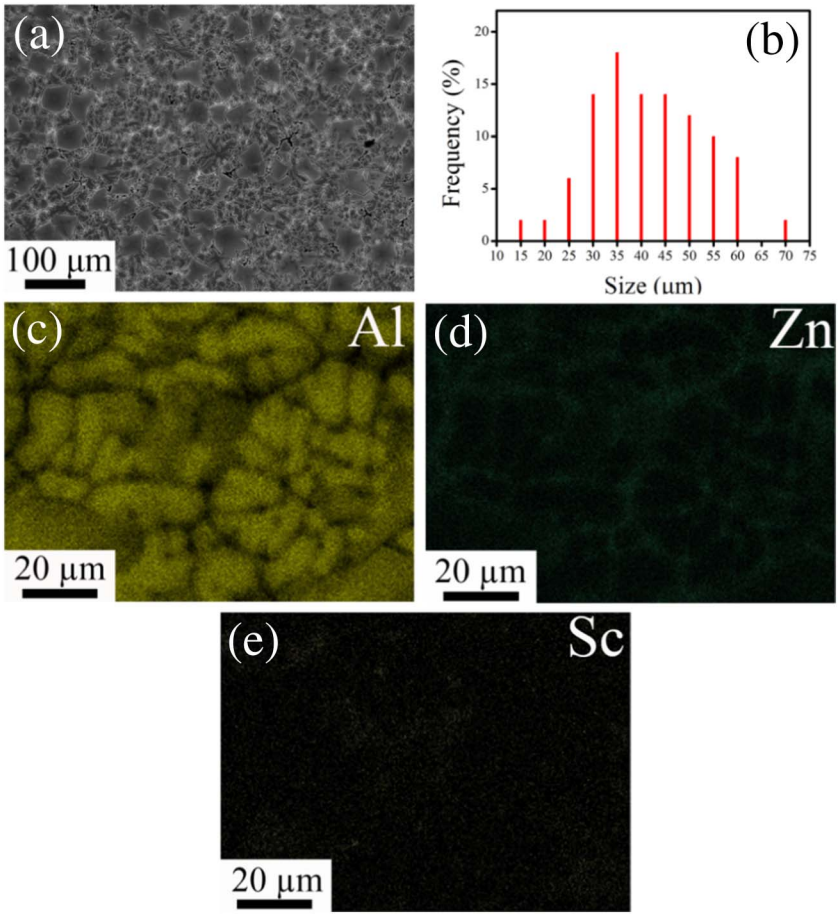

Fig. 3. (a) SEM micrograph and (b) equiaxed grain size distributions of the as-cast Al–49Zn–0.5Sc alloy. The corresponding composition mapping of Al, Zn, and Sc is shown in (c), (d), and (e), respectively.

phase, which was confirmed by previous studies to be present in as-cast Al alloys containing Sc [3]. The primary Al_3Sc phase served as a heterogeneous nucleation site for Al grains during solidification and resulted in the formation of equiaxed Al grains and significant grain refinement (Fig. 3). Heterogeneous nucleation occurs in other high-Zn-concentration Al alloys, such as TiB-containing Al–35Zn alloy [23]. The heterogeneous nucleation and constitutional supercooling influenced the nucleation and growth of the Zn phase in the equiaxed grains, which led to the different distributions, morphologies, and sizes of the Zn phase in the equiaxed grains compared with those in the dendritic grains (Fig. 5(d)).

Fig. 6 presents the SEM images of the Al–49Zn alloy after heat treatment. After heating to 300 °C for 5 h, the size and morphology of the Al grains in the Al–49Zn alloy showed no significant change (Fig. 6(a)). When the temperature was increased to 400 °C, the dendritic grains changed into equiaxed grains (Fig. 6(b)), and the average grains size was about 150 μm, according to the grain size statistics (Fig. 6(e)). Fig. 6(c) and (d) shows that the GB segregation of Zn was not obvious after heating at 400 °C for 5 h.

Fig. 7 reveals the TEM micrographs of the Al–49Zn alloy after heating at 400 °C for 5 h. The GB of the sample was several hundred nanometers wide and contained some Zn particles (Fig. 7(a)). Com-

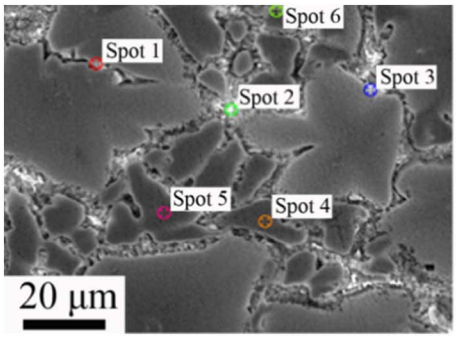

Element	Al (wt %)	Zn (wt %)	Sc (wt %)
Spot 1	48.07	50.37	1.56
Spot 2	8.02	91.62	0.06
Spot 3	35.36	63.32	1.42
Spot 4	72.62	27.14	0.25
Spot 5	73.59	26.11	0.3
Spot 6	65.84	33.95	0.22

Fig. 4. Point analysis by EDS of the as-cast Al–49Zn–0.5Sc alloy.

pared with the Zn phase in the as-cast Al–49Zn alloy (Fig. 2), that in the heat-treated alloy presented smaller sizes and higher densities (Fig. 7(b)).

Fig. 8 shows the SEM images of the Al–49Zn–0.5Sc alloy after heat treatment. After heating to 300 °C and 400 °C for 5 h, the equiaxed grains in the Al–49Zn–0.5Sc alloy underwent slight coarsening (Fig. 8(a) and (b)). When the temperature was increased to 480 °C, the dendritic grains disappeared (Fig. 8(c)). And the average equiaxed grains size of this sample was increased to approximately 55 μm, according to the grain size statistics (Fig. 8(d)).

Fig. 9 reveals the TEM micrographs of the Al–49Zn–0.5Sc alloy after heating at 400 °C for 5 h. Numerous nanoparticles and Zn phases can be observed near the GB. The nanoparticles were less than 5 nm in size and equiaxed. The selected area of diffraction revealed that the nanoparticles contained the Al_3Sc phase.

Fig. 10 displays the TEM micrographs of the Al–49Zn–0.5Sc alloy after heating at 480 °C for 5 h. The Zn phase was uniformly distributed in the Al grain after heat treatment (Fig. 10(a)). Furthermore, the Zn phase was surrounded by a high density of nanoparticles (Fig. 10(b)). Through HRTEM and FFT analyses, the nanoparticles were identified as Al_3Sc (Fig. 10(c)).

Fig. 11 shows the X-ray diffraction (XRD) patterns of the Al–49Zn and Al–49Zn–0.5Sc alloys after different heat treatments. For the Al–49Zn alloy, the Al peaks shifted toward the high-angle orientation after heating at 400 °C for 5 h. The atomic radius of Zn (0.153 nm) was smaller than that of Al (0.182 nm). Several studies showed that the lattice parameter of Al increased with decreasing Zn concentration or precipitation of the Zn phase from the Al matrix [24–26]. Thus, in the present study, as the Zn atoms dissolved in the Al lattice, the lattice parameter of the Al matrix decreased, and the Al peaks shifted toward the high-angle orientation. By contrast, no peak shifts were observed in the Al–49Zn–0.5Sc alloy during heat treatments (Fig. 11 inset).

The Al–49Zn and Al–49Zn–0.5Sc alloys exhibited different thermal stabilities (Figs. 6 and 8). The dendritic grains transformed into equiaxed grains, with an average size of 150 μm in the Al–49Zn alloy after heat treatment at 400 °C for 5 h (Fig. 6(b)). Meanwhile, the same heat treatment induced no significant changes in the morphology and size of the Al grains in the Al–49Zn–0.5Sc alloy (Fig. 8(b)). The

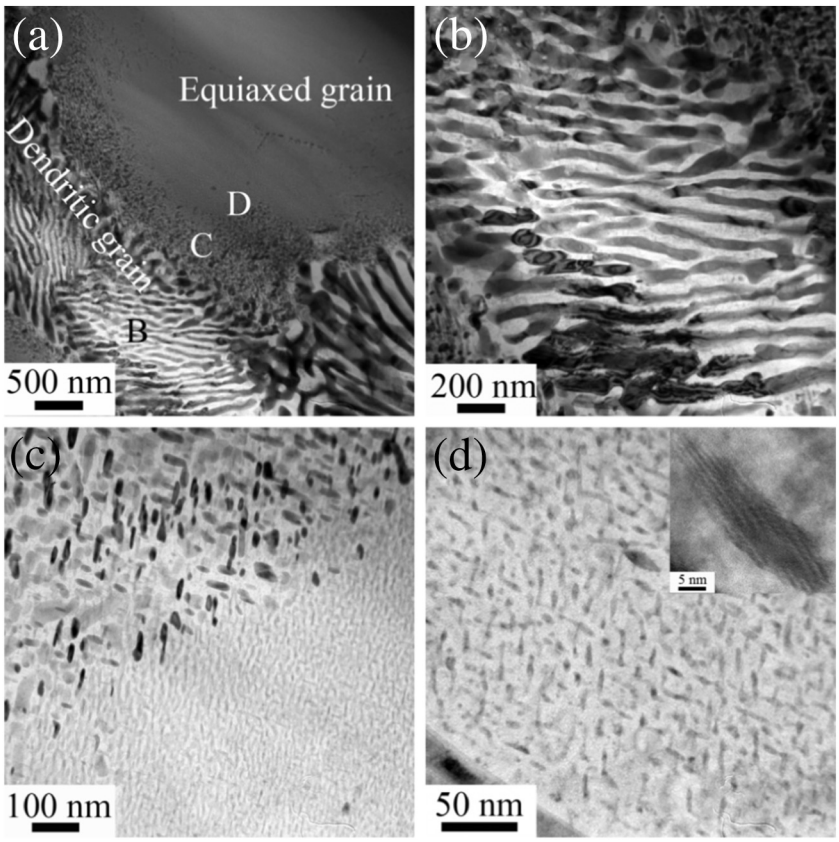

Fig. 5. TEM micrographs of the as-cast Al–49Zn–0.5Sc alloy at the (a) lower magnification and higher magnification of (b) Regions B, (c) C, and (d) D in panel (a).

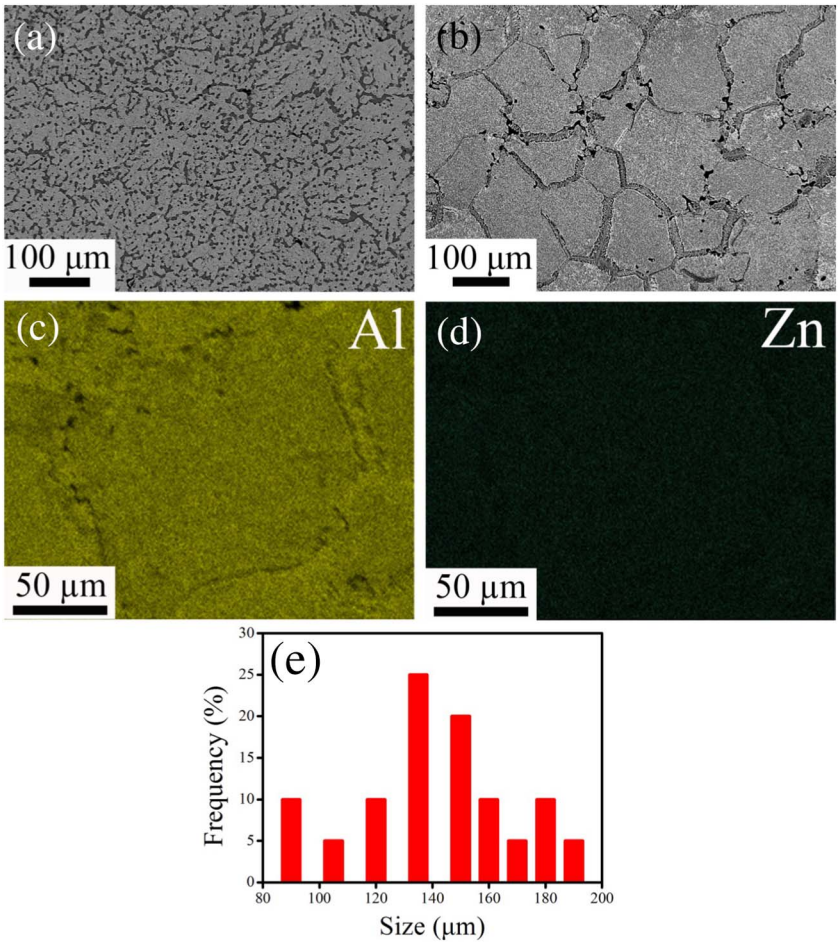

Fig. 6. (a) SEM micrographs of the Al–49Zn alloy after heating at (a) 300 °C and (b) 400 °C for 5 h. The corresponding composition mapping of Al and Zn of the Al–49Zn alloy after heating at 400 °C for 5 h is shown in (c) and (d), respectively. And (e) grain size distributions of the Al–49Zn alloy after heating at 400 °C for 5 h.

equiaxed grain size increased to approximately 59 μm in the Al–49Zn–0.5Sc alloy when the heating temperature was increased to 480 °C, which was near the solidus curve temperature of the Al–49Zn system (Fig. 8(c)).

Sc segregated near the GBs of the as-cast Al–49Zn–0.5Sc alloy, as shown by Spots 1 and 3 in Fig. 4. Heat treatment induced the precipitation of numerous Al_3Sc nanoparticles along the GBs (Fig. 9). These particles can strongly pin GBs and dislocations during annealing [27,28] and thereby prevent intense grain growth. Compared with the Al–49Zn–0.5Sc alloy, the Al–49Zn alloy possessed “cleaner” GBs (Fig. 7(a)) and presented no pinning effect derived from nanoparticles. Therefore, the Al grains in the Al–49Zn–0.5Sc alloy exhibited a higher thermal stability compared with those in the Al–49Zn alloy.

Not only the Al grains but also the Zn phase in the Al–49Zn and Al–49Zn–0.5Sc alloys demonstrated different thermal stabilities. For the Al–49Zn alloy, the following three phenomena were observed during heat treatment: 1) Zn segregation was almost eliminated, as shown by the EDS mapping (Figs. 1 and 6); 2) the size of the Zn phase in the Al grains was obviously refined (Figs. 2 and 7); and 3) the XRD peaks of Al shifted toward the high-angle orientation (Fig. 11). Obvious

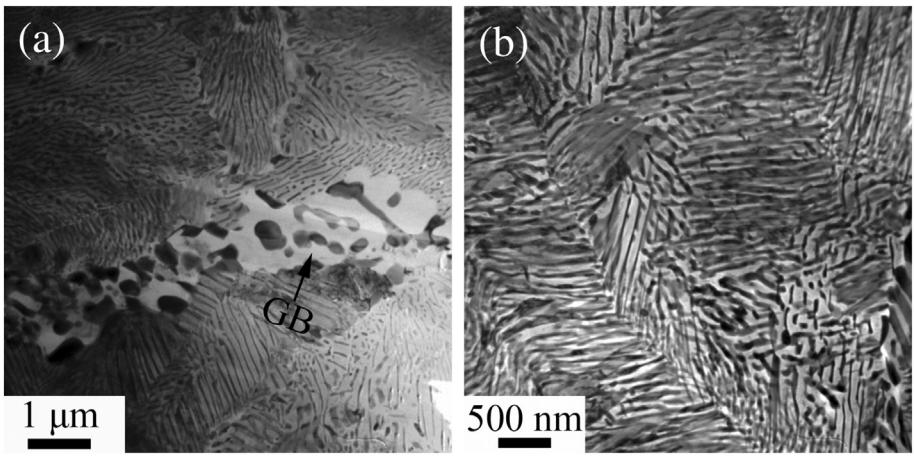

Fig. 7. TEM micrographs of the Al–49Zn alloy after heating at 400 °C for 5 h. The (a) GB and (b) grain interior are displayed.

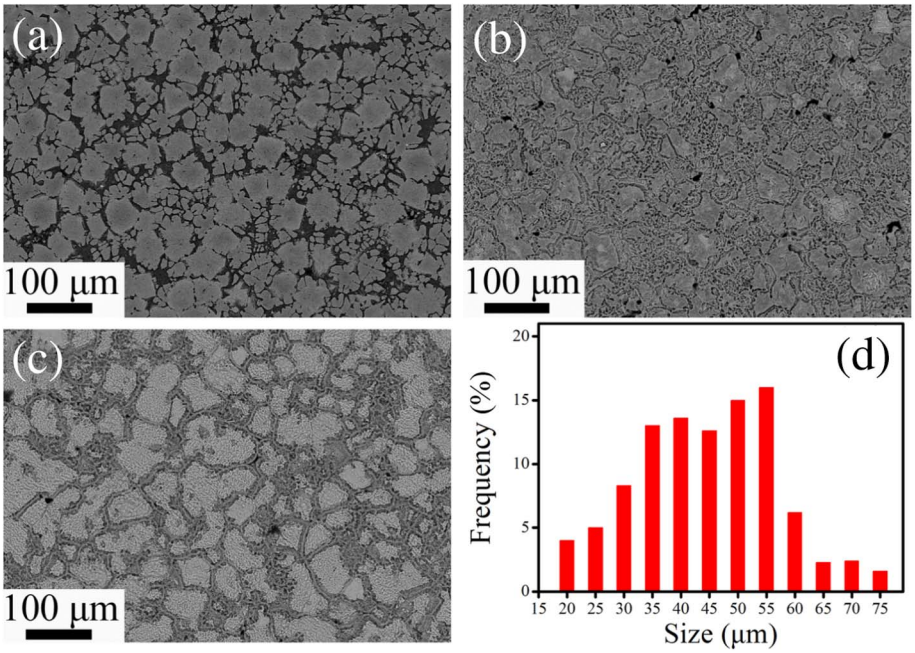

Fig. 8. SEM micrographs of the Al–49Zn–0.5Sc alloy after heating at (a) 300 °C, (b) 400 °C, and (c) 480 °C for 5 h. And (d) grain size distributions of the Al–49Zn–0.5Sc alloy after heating at 480 °C for 5 h.

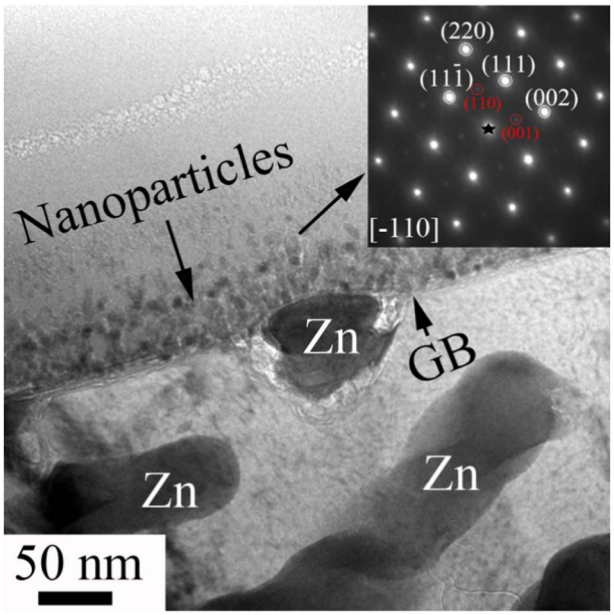

Fig. 9. TEM micrograph of the Al–49Zn–0.5Sc alloy after heating at 400 °C for 5 h. The inset shows the diffraction pattern of the selected area. The white and red numbers correspond to the planes of Al and Al_3Sc, respectively. (For interpretation of the references to colour in this figure legend, the reader is referred to the web version of this article.)

solid-solution reaction occurred in the as-cast Al–49Zn alloy during heat treatment. Furthermore, the solid-solution reaction possibly led to the uniform distribution of Zn elements and refinement of the Zn phase.

Nearly no peak shift occurred in the Al–49Zn–0.5Sc alloy during heat treatments even when the heat temperature was increased to 480 °C (Fig. 11). This phenomenon indicates that the solid-solution reaction of Zn to the Al lattice was suppressed in this alloy. As mentioned above, the growth of the Zn phase was suppressed by Sc atoms during solidification. Thus, the Zn phase in the as-cast Al–49Zn–0.5Sc alloy was surrounded by a high density of Sc atoms. A similar phenomenon was also observed in other systems. For example, Sc can be enriched at the Si/Al interface of Al–Si–Sc alloys [29], and Sc segregation at the Al_2Cu/Al matrix interfaces was characterized by using 3DAP in Al–Cu–Sc alloys [30,31].

Chen et al. [7] discovered that the growth of Al_2Cu precipitates can be inhibited by Sc atoms in the Al–Cu–Sc alloy during 250 °C annealing. Both precipitation and dissolution were affected by Sc. In this study, the solid solution of Zn atoms to the Al lattice was suppressed by the enrichment of Sc at the Zn phase/Al matrix interfaces of the Al–49Zn–0.5Sc alloy during annealing at 400 °C. When the heating temperature was increased to 480 °C, the Al_3Sc nanoparticles precipitated around the Zn phase (Fig. 10(b)). These particles also suppressed the solid-solution reaction in the Al–49Zn–0.5Sc alloy. Therefore, the Zn phase in the Al–49Zn–0.5Sc alloy showed greater thermal stability than that in the Al–49Zn alloy.

Fig. 12 shows that the hardness values of the Al–49Zn and Al–49Zn–0.5Sc alloys in their cast state were 92 and 127 HV, respectively. The hardness of the Al–49Zn alloy increased with rising heating temperature and then peaked to 152 HV at 400 °C. Then, the hardness remained stable with further increase in heating temperature. Unlike the Al–49Zn alloy, the Al–49Zn–0.5Sc alloy exhibited higher hardness stability at temperatures below 450 °C. Then, the value slightly decreased with increasing heat temperature.

The refined structures, such as fine Al grain and nanosized Zn phase in the as-cast Al–49Zn–0.5Sc alloy, increased the hardness value of this alloy compared with the as-cast Al–49Zn alloy.

For the Al–Zn system, solid-solution strengthening is the most important strengthening mechanism. For example, hardening by grain refinement, the increase in the number of dislocations, the presence of nanosized precipitates, and the softening by the decomposition of supersaturated solid solution occur simultaneously during the deformation of supersaturated binary Al–Zn alloys. The net effect of above phenomena always leads to the “work softening” exhibited by the supersaturated Al–Zn alloys [15,18,25,26,32]. Hence, the increments in solid-solution strengthening significantly enhanced the hardness of the Al–49Zn alloy after heat treatments. Meanwhile, the low-temperature (below 400 °C) heat-treated Al–49Zn–0.5Sc alloy showed nearly no hardness change due to the high microstructure stability during heat treatment. When the heating temperature exceeded 400 °C, slight softening was observed in the Al–49Zn–0.5Sc alloy because of grain

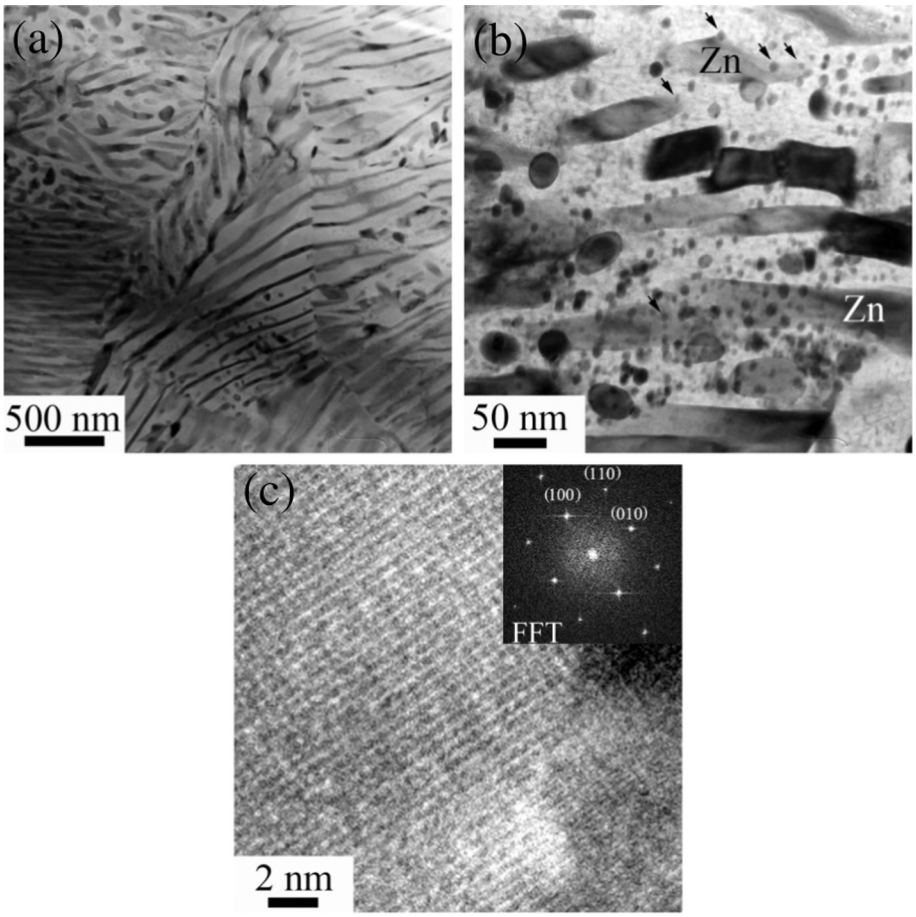

Fig. 10. TEM micrographs of the Al–49Zn–0.5Sc alloy after heating at 480 °C for 5 h at (a) lower magnification, (b) higher magnification, and (c) under HRTEM of the nanoparticles in panel (b). The arrows in panel (b) denote the nanoparticles.

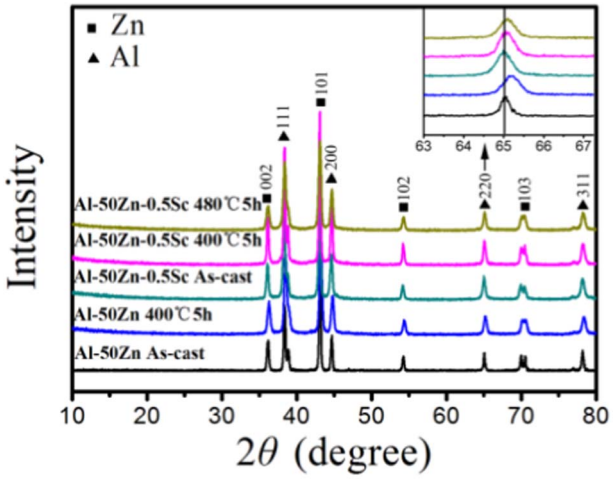

Fig. 11. XRD of the as-cast and heat-treated Al–49Zn and Al–49Zn–0.5Sc alloys under different heating temperatures.

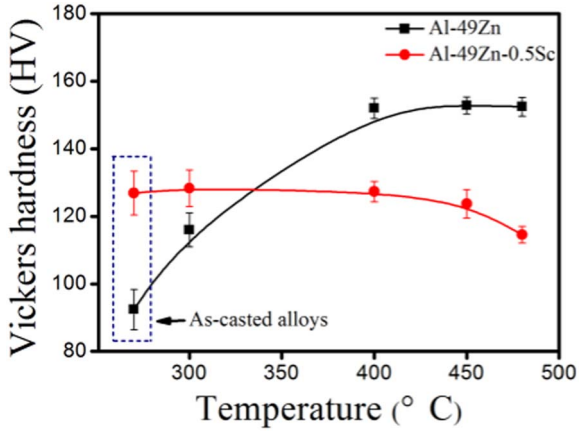

Fig. 12. Variation in Vickers hardness of the as-cast and heat-treated Al–49Zn and Al–49Zn–0.5Sc alloys after heating at different temperatures.

coarsening.

4. Conclusions

The effect of Sc addition on the solidification, thermal stability, and hardness of a high-Zn-concentration Al alloy were investigated. The following conclusions were reached:

(1) The addition of 0.5Sc to the Al–49Zn alloy caused the dendritic substructure to change into a bimodal structure containing dendritic and equiaxed grains in the cast state. Furthermore, 0.5Sc addition led to the significant grain refinement and changes in distribution, morphology, and size of the Zn phase in the Al–49Zn alloy.

(2) Compared with the Al–49Zn alloy, the Al–49Zn–0.5Sc alloy showed a higher thermal stability. In addition, the grain size of the Al–49Zn–0.5Sc alloy was approximately 59 μm after heating at 480 °C for 5 h. The nanoscale Al_3Sc precipitates strongly pinned the GBs and prevented grain growth during annealing. An obvious solid-solution reaction occurred in the Al–49Zn alloy during heat

treatment. Meanwhile, the solid solution of Zn atoms to the Al lattice was suppressed by the addition of Sc in the Al–49Zn–0.5Sc alloy during heat treatment.

(3) Both the finer Al grain size and nanosized Zn phase improved the hardness of the as-cast Al–49Zn–0.5Sc alloy compared with the as-cast Al–49Zn alloy. After heat treatment, the increase in solid-solution strengthening enhanced the hardness of the Al–49Zn alloy. Minor hardness changes occurred in the Al–49Zn–0.5Sc alloy because of the high thermal stability of this alloy.

Acknowledgements

This work was funded by Research Program of Science and Technology of Guangxi (No. GKAB16380021), the Guangxi 'Bagui' Teams for Innovation and Research, Research Program of College Science and Technology of Hebei Province (No. QN2015236), and Collaborative Innovation Center for Exploration of Hidden Nonferrous Metal Deposits and Development of New Materials in Guangxi (GXYSXTZX2016-II-2).

References

[1] C. Xu, W.L. Xiao, S. Hanada, H. Yamagata, C.L. Ma, The effect of scandium addition on microstructure and mechanical properties of Al–Si–Mg alloy: a multi-refinement modifier, Mater. Charact. 110 (2015) 160–169.
[2] W.D. Zhang, Y. Liu, J. Yang, J.Z. Dang, H. Xu, Z.M. Du, Effects of Sc content on the microstructure of As–Cast Al–7 wt% Si alloys, Mater. Charact. 66 (2012) 104–110.
[3] S.A. Zhou, Z. Zhang, M. Li, D.J. Pan, H.L. Su, X.D. Du, P. Li, Y.C. Wu, Effect of Sc on microstructure and mechanical properties of as-cast Al–Mg alloys, Mater. Des. 90 (2016) 1077–1084.
[4] F.C. Liu, Z.Y. Ma, F.C. Zhang, High strain rate superplasticity in a micro-grained Al–Mg–Sc alloy with predominant high angle grain boundaries, J. Mater. Sci. Technol. 28 (2012) 1025–1030.
[5] F.C. Liu, Z.Y. Ma, L.Q. Chen, Low-temperature superplasticity of Al–Mg–Sc alloy produced by friction stir processing, Scr. Mater. 60 (2009) 968–971.
[6] O.N. Senkov, M.R. Shagiev, S.V. Senkova, D.B. Miracle, Precipitation of Al_3(Sc, Zr) particles in an Al–Zn–Mg–Cu–Sc–Zr alloy during conventional solution heat treatment and its effect on tensile properties, Acta Mater. 56 (2008) 3723–3738.
[7] B.A. Chen, L. Pan, R.H. Wang, G. Liu, P.M. Cheng, L. Xiao, J. Sun, Effect of solution treatment on precipitation behaviors and age hardening response of Al–Cu alloys with Sc addition, Mater. Sci. Eng. A 530 (2011) 607–617.
[8] T. Liu, C.N. He, G. Li, X. Meng, C.S. Shi, N.Q. Zhao, Microstructural evolution in Al–Zn–Mg–Cu–Sc–Zr alloys during short–time homogenization, Int. J. Miner. Metall. Mater. 5 (2015) 516–523.
[9] J. Liu, P. Yao, N.Q. Zhao, C.S. Shi, H.J. Li, X. Li, D.S. Xi, S. Yang, Effect of minor Sc and Zr on recrystallization behavior and mechanical properties of novel Al–Zn–Mg–Cu alloys, J. Alloys Compd. 657 (2016) 717–725.
[10] F.C. Liu, P. Xue, Z.Y. Ma, Microstructural evolution in recrystallized and unrecrystallized Al-Mg-Sc alloys during superplastic deformation, Mater. Sci. Eng. A 547 (2012) 55–63.
[11] Y.Y. Peng, Z.M. Yin, X.F. Lei, Q.L. Pan, Z.B. He, Microstructure and properties of friction stir welded joints of Al–Mg–Sc alloy plates, Rare Metal Mater. Eng. 40 (2011) 201–205.
[12] N. Kumar, R.S. Mishra, Thermal stability of friction stir processed ultrafine grained Al–Mg–Sc alloy, Mater. Charact. 74 (2012) 1–10.
[13] H.F. Huang, F. Jiang, J. Zhou, L.L. Wei, M.C. Zhong, X.T. Liu, Hot deformation behavior and microstructural evolution of as-homogenized Al–6Mg–0.4Mn–0.25Sc–0.1Zr alloy during compression at elevated temperature, J. Alloys Compd. 644 (2015) 862–872.
[14] S.S. Shin, K.M. Lim, I.M. Park, Characteristics and microstructure of newly designed Al–Zn–based alloys for the die-casting process, J. Alloys Compd. 671 (2016) 517–526.
[15] A. Alhamidi, K. Edalati, Z. Horita, S. Hirosawa, K. Matsuda, D. Terada, Softening by severe plastic deformation and hardening by annealing of aluminum–zinc alloy: significance of elemental and spinodal decompositions, Mater. Sci. Eng. A 610 (2014) 17–27.
[16] C.Y. Liu, B. Qu, Z.Y. Ma, M.Z. Ma, R.P. Liu, Recrystallization, precipitation, and resultant mechanical properties of rolled Al–Zn alloy after aging, Mater. Sci. Eng. A 657 (2016) 284–290.
[17] C.Y. Liu, M.Z. Ma, R.P. Liu, K. Luo, Evaluation of microstructure and mechanical properties of Al–Zn alloy during rolling, Mater. Sci. Eng. A 654 (2016) 436–441.
[18] C.Y. Liu, L. Yu, M.Z. Ma, R.P. Liu, Z.Y. Ma, Dynamic precipitation of Al–Zn alloy during rolling and accumulative roll bonding, Philos. Mag. Lett. 95 (2015) 539–546.
[19] X. Sauvage, M.Y. Murashkin, B.B. Straumal, E.V. Bobruk, R.Z. Valiev, Ultrafine grained structures resulting from SPD–induced phase transformation in Al–Zn alloys, Adv. Eng. Mater. 17 (2015) 1821–1827.
[20] C.Y. Liu, B. Zhang, P.F. Yu, R. Jing, M.Z. Ma, R.P. Liu, Microstructures and mechanical properties of Al/Zn composites prepared by accumulative roll bonding and heat treatment, Mater. Sci. Eng. A 580 (2013) 36–40.
[21] B. Li, Q.L. Pan, Z.M. Yin, Microstructural evolution and constitutive relationship of Al–Zn–Mg alloy containing small amount of Sc and Zr during hot deformation based on Arrhenius-type and artificial neural network models, J. Alloys Compd. 584 (2014) 406–416.
[22] Y. Karamazi, Ü. Bayram, P. Ata, S. Akszöz, K. Keşlioğlu, N. Maraşli, Dependence of microstructural, mechanical and electrical properties on growth rates in directional solidified Zn − Al − Bi eutectic alloy, Trans. Nonferrous Metals Soc. China 26 (2016) 2320–2335.
[23] S.S. Shin, G.Y. Yeom, T.Y. Kwak, I.M. Park, Microstructure and mechanical properties of TiB-containing Al–Zn binary alloys, J. Mater. Sci. Technol. 32 (2016) 653–659.
[24] B.B. Straumal, B. Baretzky, A.A. Mazilkin, F. Phillipp, O.A. Kogtenkova, M.N. Volkov, R.Z. Valiev, Formation of nanograined structure and decomposition of supersaturated solid solution during high pressure torsion of Al–Zn and Al–Mg alloys, Acta Mater. 52 (2004) 4469–4478.
[25] A.A. Mazilkin, B.B. Straumal, E. Rabkin, B. Baretzky, S. Enders, S.G. Protasova, O.A. Kogtenkova, R.Z. Valiev, Softening of nanostructured Al–Zn and Al–Mg alloys after severe plastic deformation, Acta Mater. 54 (2006) 3933–3939.
[26] A.A. Mazilkin, B.B. Straumal, M.V. Borodachenkova, R.Z. Valiev, O.A. Kogtenkova, B. Baretzky, Gradual softening of Al–Zn alloys during high-pressure torsion, Mater. Lett. 84 (2012) 63–65.
[27] Y. Deng, G.F. Xu, Z.M. Yin, X.F. Lei, J.W. Huang, Effects of Sc and Zr microalloying additions on the recrystallization texture and mechanism of Al–Zn–Mg alloys, J. Alloys Compd. 580 (2013) 412–426.
[28] E. Avtokratova, O. Sitdikov, M. Markushev, R. Mulyukov, Extraordinary high-strain rate superplasticity of severely deformed Al–Mg–Sc–Zr alloy, Mater. Sci. Eng. A 538 (2012) 386–390.
[29] M. Fatih Kilicaslan, W.R. Lee, T.H. Lee, Y. Sohn, S.J. Hong, Effect of Sc addition on the microstructure and mechanical properties of as-atomized and extruded Al–20Si alloys, Mater. Lett. 71 (2012) 164–167.
[30] B.A. Chen, G. Liu, R.H. Wang, J.Y. Zhang, L. Jiang, J.J. Song, J. Sun, Effect of interfacial solute segregation on ductile fracture of Al–Cu–Sc alloys, Acta Mater. 61 (2013) 1676–1690.
[31] L. Jiang, J.K. Li, G. Liu, R.H. Wang, B.A. Chen, J.Y. Zhang, J. Sun, M.X. Yang, G. Yang, J. Yang, X.Z. Cao, Length-scale dependent microalloying effects on precipitation behaviors and mechanical properties of Al–Cu alloys with minor Sc addition, Mater. Sci. Eng. A 637 (2015) 139–154.
[32] M. Borodachenkova, F. Barlat, W. Wen, A. Bastos, J.J. Grácio, A microstructure-based model for describing the material properties of Al–Zn alloys during high pressure torsion, Int. J. Plast. 68 (2015) 150–163.